Free Radical Biology and Medicine 255 (2026) 730–743

Contents lists available at ScienceDirect

Free Radical Biology and Medicine

journal homepage: www.elsevier.com/locate/freeradbiomed

# Proximal tubular EZH2 inhibits diabetic kidney disease by suppressing SHC1-mediated oxidative stress

Qiming Xu [a,b,c,d,1], Pinglan Lin [a,b,c,1], Sijun Chen [e,1], Jianrao Lu [d], Lin Li [f], Reza Moghadasali [g], Xuejun Yang [a,b,c], Jing Hu [d,***], Ming Wu [a,b,c,**], Dongping Chen [a,b,c,*]

[a] Department of Nephrology, Shanghai Shuguang Hospital Affiliated to Shanghai University of Traditional Chinese Medicine, PR China
[b] TCM Institute of Kidney Disease of Shanghai University of Traditional Chinese Medicine, PR China
[c] Key Laboratory of Liver and Kidney Diseases, Ministry of Education, Shanghai Key Laboratory of Traditional Chinese Clinical Medicine, PR China
[d] Department of Nephrology, Shanghai Seventh People's Hospital Affiliated to Shanghai University of Traditional Chinese Medicine, PR China
[e] Department of Nephrology, Yangpu Hospital, School of Medicine, Tongji University, Shanghai, 200090, PR China
[f] Department of Nephrology, Shanghai Changzheng Hospital (Second Affiliated Hospital of Naval Medical University), Shanghai, PR China
[g] Department of Stem Cells and Developmental Biology, Cell Science Research Center, Royan Institute for Stem Cell Biology and Technology, ACECR, Tehran, Iran

ARTICLE INFO

*Keywords:*
EZH2
Diabetic kidney disease
Renal tubule
SHC1
Oxidative stress

ABSTRACT

Diabetic kidney disease (DKD) represents one of the most severe complications of diabetes. Although EZH2 (Enhancer of Zeste Homolog 2) has been implicated in renal injury and diabetes, its specific function within renal tubular cells in DKD remains unclear. Here, we explored the role and downstream mechanism of tubular EZH2 in DKD progression.

Renal EZH2 expression was significantly upregulated in DKD. Single-nucleus RNA sequencing and immunofluorescence analyses verified that such elevation was restricted to proximal tubular epithelial cells. Conversely, tubular-specific deletion of *Ezh2* exacerbated renal dysfunction and fibrosis in DKD mice. *In vitro* gain- and loss-of-function experiments in high glucose-stimulated HK2 cells further validated that EZH2 plays a renoprotective role under diabetic conditions. Mechanistically, we demonstrated that EZH2 epigenetically suppresses the pro-oxidative mediator SHC1. In the DKD mouse model, renal SHC1 protein abundance was markedly increased upon tubular *Ezh2* knockout, accompanied by reduced levels of antioxidant enzymes SOD1 and SOD2, significantly elevated MDA, and depleted GSH. Consistent with these *in vivo* observations, *in vitro* functional assays further validated that EZH2 epigenetically downregulates SHC1 and alleviates such oxidative stress perturbations. Finally, we verified that SHC1 inhibition rescues the exacerbated fibrotic response and oxidative damage triggered by pharmacological EZH2 suppression under high-glucose conditions.

In conclusion, tubular EZH2 protects against DKD via inhibiting SHC1-driven oxidative stress.

## 1. Introduction

Diabetic kidney disease (DKD), a major complication of diabetes, is the leading cause of end-stage renal disease (ESRD) in developed nations [1,2]. Beyond significantly compromising patients' quality of life, DKD imposes a substantial economic burden on healthcare systems globally [3]. Renal tubules play a crucial role in maintaining kidney function [4]. In DKD, tubular injury emerges as an early and prominent pathological feature, often preceding glomerular damage [4]. Tubular epithelial cells are highly vulnerable to diabetes-related metabolic stresses, such as hyperglycemia, hyperlipidemia, and oxidative stress [5]. Such injury disrupts normal tubular reabsorption and secretion, activates

* Corresponding author. Department of Nephrology, Shuguang Hospital Affiliated to Shanghai University of Traditional Chinese Medicine, No.528 Zhangheng Road, Pudong District, Shanghai, 201203, PR China.
** Corresponding author. Department of Nephrology, Shuguang Hospital Affiliated to Shanghai University of Traditional Chinese Medicine, No.528 Zhangheng Road, Pudong District, Shanghai, 201203, PR China.
*** Corresponding author.
*E-mail addresses:* hu12340714@163.com (J. Hu), mingwunl@126.com (M. Wu), 13764362569@163.com (D. Chen).
[1] These authors contributed equally to this paper.

https://doi.org/10.1016/j.freeradbiomed.2026.08.019
Received 7 January 2026; Received in revised form 21 July 2026; Accepted 8 August 2026
Available online 10 August 2026
0891-5849/© 2026 Published by Elsevier Inc.

inflammatory pathways, and promotes renal fibrosis, collectively contributing to the progressive decline in renal function [6,7]. A deeper understanding of the molecular basis of tubular injury in DKD is therefore essential for developing effective treatments.

EZH2 (Enhancer of Zeste Homolog 2) has emerged as a critical regulator in the pathogenesis of various kidney diseases, including renal fibrosis, acute kidney injury, and DKD [8]. Molecularly, EZH2 serves as the catalytic subunit of the polycomb repressive complex 2 (PRC2) and mediates transcriptional repression through histone H3 lysine 27 trimethylation (H3K27me3) [9]. While EZH2 promotes fibrosis in obstructive models, it appears to exert protective effects in the diabetic environment by suppressing oxidative stress in podocytes and inhibiting inflammatory responses in mesangial cells [10–12]. However, its specific role and downstream targets within the renal tubular compartment under diabetic stress remain to be fully elucidated.

SHC1 (Src homology 2 domain–containing transforming protein 1) is an adaptor protein known to participate in redox-sensitive signaling pathways that stimulate reactive oxygen species (ROS) production and subsequent cellular injury [13]. Genetic or pharmacological inhibition of SHC1 confers protective effects against DKD by alleviating oxidative stress in both podocytes and renal tubular epithelial cells [14–16]. While previous studies have validated the protective role of SHC1 suppression in diabetic renal injury, the upstream regulatory mechanisms governing SHC1 activity remain largely uncharacterized. Accumulating evidence indicates that SHC1 expression is tightly modulated by epigenetic modifications, including DNA and histone methylation [14,17,18]. Given the established role of EZH2 in repressing oxidative stress [10,19], we hypothesized that tubular EZH2 ameliorates diabetic kidney injury, at least partially, via epigenetic repression of SHC1-mediated oxidative stress.

The objective of this study was to elucidate the specific role and underlying mechanism of tubular EZH2 in DKD. Using tubular-specific *Ezh2* conditional knockout mice and *in vitro* models of renal tubular epithelial cells, we investigated how tubular EZH2 influences disease progression in diabetic kidney injury.

## 2. Results

### 2.1. EZH2 is up-regulated in the proximal tubules of diabetic kidneys

Western blot analysis showed a significant upregulation of EZH2 and H3K27me3 in the kidneys of streptozotocin (STZ)-induced diabetic mice compared to controls (Fig. 1A–B). Analysis of the Ju CKD Tublnt database revealed a negative correlation between renal EZH2 expression and glomerular filtration rate (GFR), and a positive correlation with serum creatinine levels in patients with diabetic kidney disease (DKD) (Fig. 1C).

Transcriptome data from human DKD samples (GSE30122) indicated that *EZH2* mRNA was specifically upregulated in DKD tubuli, but not in glomeruli, compared to controls (Fig. 1D). Interrogation of a public single-nucleus RNA sequencing dataset (https://humphreyslab.com/SingleCell/) revealed predominant *EZH2* expression in tubular cells across various segments, with minimal expression in glomerular cells (podocytes and mesangial cells) in both human control and DKD kidneys (Fig. 1E–F). Notably, EZH2 expression was markedly elevated in injured proximal tubular cells (VCAM1+ proximal tubular cells) in human DKD kidneys compared to controls (Fig. 1F). This specific upregulation of EZH2 in proximal tubules of diabetic mouse kidneys was further confirmed by co-immunofluorescence staining with LRP2, a proximal tubular marker (Fig. 1G).

Collectively, these findings suggest a potential role for tubular EZH2 in DKD pathogenesis.

### 2.2. EZH2 inhibits fibrotic responses in high glucose-stimulated renal epithelial cells

In HK2 human renal proximal tubular epithelial cells, high glucose stimulation elevated the expression of EZH2, H3K27me3, and the fibrotic markers fibronectin, vimentin, α-smooth muscle actin (α-SMA), and Snail (Fig. 2A–D). Pharmacological inhibition of EZH2 with 3DZNeP reduced EZH2 and H3K27me3 levels but paradoxically enhanced the expression of these fibrotic markers in high glucose-stimulated HK2 cells (Fig. 2A–D). Conversely, adenovirus-mediated overexpression of EZH2 increased EZH2 and H3K27me3 levels and concurrently suppressed the high glucose-induced expression of fibronectin, vimentin, α-SMA, and Snail (Fig. 2E–H).

These results demonstrate that EZH2 exerts an anti-fibrotic effect in renal epithelial cells under high glucose conditions.

### 2.3. Tubular-specific deletion of EZH2 exacerbates renal injury and systemic glucose intolerance in STZ-induced diabetic mice

Tubular-specific Ezh2 knockout mice were generated by crossing *Ezh2* floxed mice with Cdh16-Cre mice (Fig. 3A). Histological analysis via H&E staining revealed aggravated renal damage in diabetic mice, which was more pronounced in *Ezh2* knockout diabetic mice, characterized by enhanced tubular dilation, tubular epithelial cell atrophy, and interstitial inflammation (Fig. 3B). Diabetic mice exhibited significantly increased levels of blood urea nitrogen (BUN), serum creatinine (Scr), urine albumin-to-creatinine ratio (uACR), and kidney-to-body weight ratio compared to non-diabetic controls (Fig. 3C). Tubular deletion of *Ezh2* in diabetic mice led to a further significant increase in Scr, whereas no significant changes were observed in BUN, uACR, or kidney-to-body weight ratio (Fig. 3C).

Systemic glucose metabolism, assessed by pyruvate, insulin, and glucose tolerance tests, was impaired in diabetic mice (Fig. 3D–E). Tubular *Ezh2* deletion exacerbated this systemic glucose intolerance, as indicated by increased area under the curve (AUC) in these tests (Fig. 3D–E).

These findings indicate that tubular EZH2 confers protection against hyperglycemia-induced renal injury and systemic glucose metabolism.

### 2.4. Tubular deletion of EZH2 aggravates renal fibrosis in diabetic mice

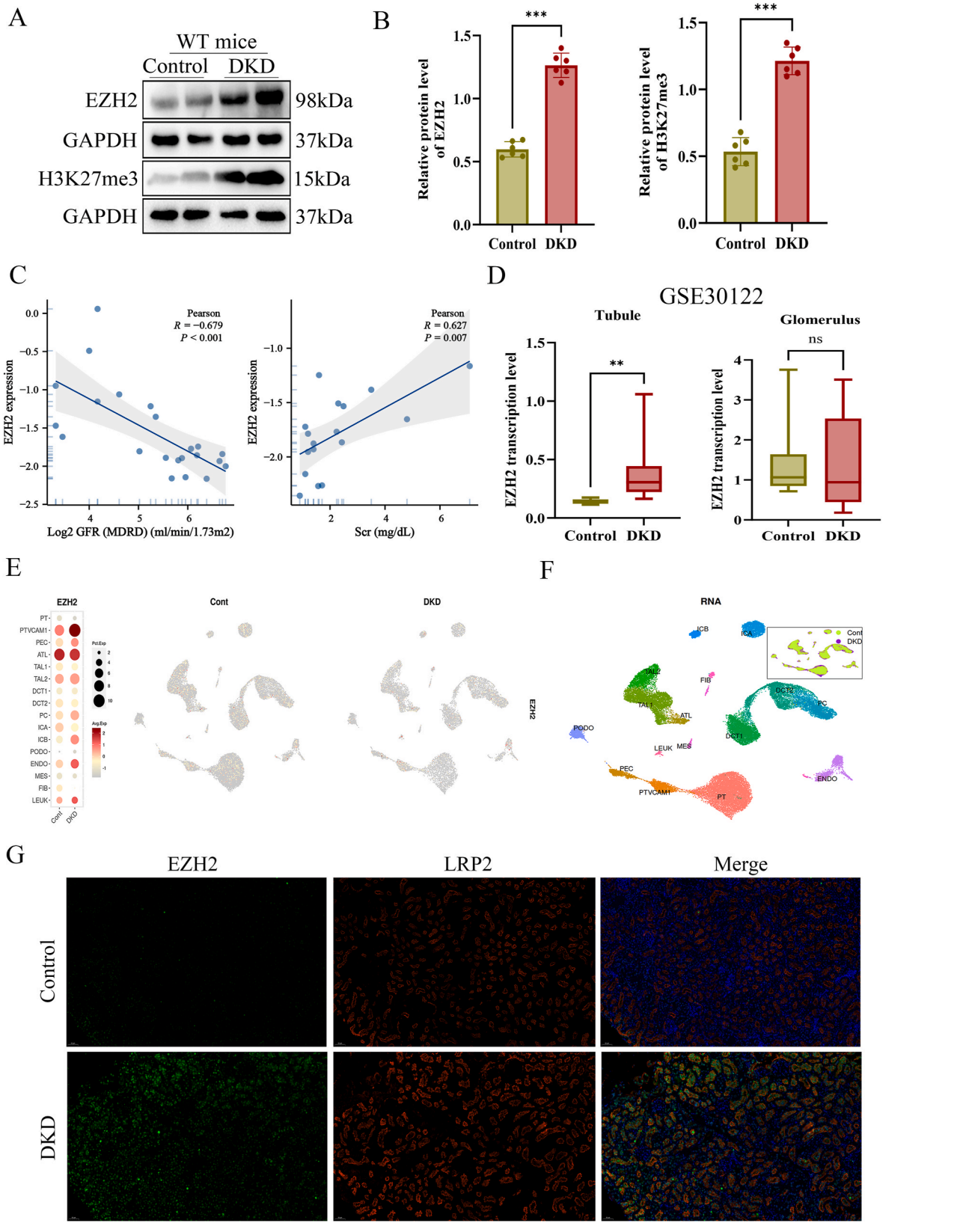
Consistent with the genetic model, Western blot analysis confirmed the downregulation of EZH2 and H3K27me3 in the kidneys of diabetic *Ezh2* CKO mice (Fig. 4A–B). The expression of fibrotic markers, including fibronectin, vimentin, α-SMA, and Snail, was increased, while the epithelial marker E-cadherin was decreased, in the kidneys of *Ezh2* knockout diabetic mice compared to wild-type diabetic controls (Fig. 4C–D).

These results demonstrate that tubular EZH2 attenuates renal fibrosis in the context of diabetes.

### 2.5. Tubular deletion of EZH2 exacerbates oxidative stress in diabetic kidneys

RNA sequencing was performed to elucidate the downstream mechanisms of tubular EZH2. Comparison between DKD/*Ezh2* WT and DKD/*Ezh2* CKO groups identified 303 differentially expressed genes, with 95 up-regulated and 208 down-regulated (Fig. 5A). Given EZH2's role as a transcriptional repressor, we focused on the up-regulated genes. Among the top 10, three (*Shc1*, *Gdf15*, and *Ugt1a10*) have reported links to oxidative stress (Fig. 5B) [13,20,21]. Subsequent qPCR validation confirmed that only *Shc1* mRNA was significantly upregulated in *Ezh2* CKO kidneys (Fig. 5C), a finding corroborated at the protein level by Western blot (Fig. 5D and F).

Since SHC1 is a known promoter of oxidative stress [13], we assessed its functional consequences. Tubular *Ezh2* deletion in diabetic kidneys




(caption on next page)

**Fig. 1.** EZH2 is up-regulated in the proximal tubules of diabetic kidneys
(A-B) Western blot analysis and quantification of EZH2 and H3K27me3 protein expression in kidney tissues from control and STZ-induced diabetic mice. (C) Correlation analysis between renal *EZH2* expression and GFR or serum creatinine (Scr) levels in patients with diabetic kidney disease (DKD) using the Ju CKD Tublnt database. (D) RNA-seq analysis of public datasets (GSE30122) revealing *EZH2* expression in tubule or glomerulus of healthy or DKD human kidneys. (E) UMAP plot of integrated snRNA-seq dataset with annotation by cell type and disease condition. PT: proximal tubules, PTVCAM1: VCAM1(+) proximal tubule, PEC: Parietal Epithelial Cells ATL: ascending thin limb, TAL1: CLDN16(−) thick ascending limb, TAL2: CLDN16(+) thick ascending limb, FIB: Fibroblasts, ICA: Type A intercalated cell of collecting duct, ICB: Type B intercalated cell of collecting duct, LEUK: Leukocytes, DCT1: early distal convoluted tubule, DCT2: late distal convoluted tubule, PC: principal cells, PODO: podocytes, MES: Mesangial cells, and ENDO: Endothelial cells. (F) snRNA-seq analysis of a public dataset revealing *EZH2* expression in different cellular groups in human DKD kidneys. (G) Immunofluorescence staining (200× magnification) of EZH2 (green) with tubular marker LRP2 (red) in diabetic mouse kidney sections. Merged images with DAPI (blue). One representative of at least three independent experiments is shown. Data represent mean ± SD. Ns represent not significant. $^{**}p < 0.01$. $^{***}p < 0.001$.

led to decreased protein levels of the antioxidant enzymes SOD1 and SOD2 (Fig. 5E–F), reduced glutathione (GSH) levels, and increased malondialdehyde (MDA) content, a marker of lipid peroxidation (Fig. 5G).

These data suggest that tubular EZH2 mitigates oxidative stress in DKD, potentially through the repression of *SHC1*.

### 2.6. EZH2 attenuates oxidative stress in high glucose-stimulated renal epithelial cells

In high glucose-stimulated HK2 cells, EZH2 inhibition by 3DZNeP increased SHC1 expression, decreased SOD1 and SOD2 levels (Fig. 6A–B), elevated reactive oxygen species (ROS) concentration, and reduced GSH concentration (Fig. 6C).

Conversely, EZH2 overexpression decreased SHC1 expression, increased SOD1 and SOD2 levels (Fig. 6D–E), reduced ROS, and elevated GSH (Fig. 6F). Furthermore, CUT&Tag–qPCR analysis revealed significant enrichment of both EZH2 and its associated repressive histone mark H3K27me3 at the *SHC1* promoter in high glucose–stimulated HK-2 cells, with EZH2 overexpression further enhancing these enrichments (Fig. 6G and H).

Collectively, these findings demonstrate that EZH2 inhibits oxidative stress in renal epithelial cells under high glucose conditions through a mechanism involved with epigenetic repression of *SHC1*.

### 2.7. EZH2-mediated anti-fibrotic effects are dependent on suppression of SHC1

Next, we examined whether the pro-fibrotic effects of EZH2 inhibition were mediated by SHC1. In high glucose-stimulated HK2 cells, the SHC1 inhibitor idebenone reversed the pro-fibrotic effects of 3DZNeP, as evidenced by suppressed expression of fibronectin, vimentin, and α-SMA (Fig. 7A–B).

Idebenone also counteracted the pro-oxidant effects of 3DZNeP, shown by reduced SHC1 expression, increased SOD1/SOD2 levels (Fig. 7C–D), normalized GSH depletion, and attenuated ROS overproduction (Fig. 7E–G).

These results indicate that the pro-oxidant regulator SHC1 mediates the anti-fibrotic effects of EZH2 in renal epithelial cells under high glucose stress.

## 3. Discussion

Previous studies have established a protective role for EZH2 in hyperglycemia-induced glomerular injury [10,11]. However, its specific function in tubular pathology during diabetic kidney disease (DKD) remained unclear. Our study demonstrates that EZH2 is predominantly expressed in renal tubules and is upregulated under diabetic conditions. We identified a crucial protective role for tubular EZH2 in DKD pathogenesis. Functionally, EZH2 inhibited fibrotic responses in high glucose-stimulated renal proximal tubular epithelial cells. Furthermore, tubular-specific deletion of *Ezh2* exacerbated renal function decline, fibrosis, histological damage, and systemic glucose metabolism in STZ-induced diabetic mice.

A key finding of our study is the inhibitory effect of EZH2 on fibrotic responses in renal epithelial cells under high glucose conditions. EZH2 overexpression suppressed the expression of fibrotic markers, whereas its inhibition enhanced fibrotic responses in high glucose stimulated renal epithelial cells, suggesting EZH2 as a potential therapeutic target for mitigating renal tubulointerstitial fibrosis in DKD. In addition, EZH2 appears to exert protective effects in the glomerular compartments in DKD: it suppresses oxidative stress in podocytes [10], and inhibits TGF-β-induced fibrotic and inflammatory responses in mesangial cells [11]. Renal fibrosis is a hallmark of disease progression in chronic kidney diseases, including DKD [22]. Interestingly, EZH2 has been reported to promote renal fibrosis in other CKD models, such as those induced by obstructive nephropathy, ischemia-reperfusion injury, or nephrotoxins [8]. This context-dependent role underscores the necessity of tailoring EZH2-targeted therapies to the specific etiology of CKD.

Mechanistically, we found that EZH2 exerts its protective effects primarily through the inhibition of oxidative stress. While EZH2 has previously been shown to protect podocytes from hyperglycemia-induced injury via regulation of the antioxidant inhibitor thioredoxin-interacting protein (TxnIP) [10], our study newly identifies SHC1 as a downstream target of EZH2 in the tubular response to diabetic stress. SHC1 is a recognized regulator of oxidative stress, and its activation can promote ROS production and subsequent cellular damage [13]. Previous studies indicate that SHC1 inhibition is protective in DKD by reducing oxidative injury in tubular cells and podocytes [14–16]. However, the upstream regulation of SHC1 in DKD was not fully understood. Our results demonstrate that tubular deletion of *Ezh2* increased *Shc1* expression and oxidative stress markers, whereas EZH2 overexpression suppressed them. Furthermore, we identified EZH2 and H3K27me3 occupancy at the SHC1 promoter in high-glucose–stimulated HK-2 cells, with enrichment further enhanced upon EZH2 overexpression. Importantly, the SHC1 inhibitor idebenone reversed both the pro-fibrotic and pro-oxidant effects induced by EZH2 inhibition in high glucose-stimulated tubular cells. These findings collectively suggest that epigenetic suppression of SHC1-mediated oxidative stress is a central mechanism through which EZH2 protects against tubular injury in DKD.

In this study, tubular-specific *Ezh2* deletion exacerbated systemic glucose intolerance in diabetic mice, as evidenced by impaired pyruvate, insulin, and glucose tolerance tests. The proximal tubule plays a central role in gluconeogenesis, accounting for approximately 40% of systemic glucose production in the fasting state [23]. EZH2 may directly or indirectly influence tubular gluconeogenic enzyme expression, thereby affecting systemic glucose homeostasis. This is an interesting research topic warranting further investigation.

Regarding the aggravated renal injury in DKD mice, we propose that this phenotype reflects a combined effect of direct tubular *Ezh2* deficiency and secondary insults resulting from the deteriorated systemic metabolic state. Importantly, our *in vitro* experiments in HK 2 cells using EZH2 overexpression and inhibition demonstrated that EZH2 directly inhibits fibrosis and oxidative stress under high glucose conditions, independent of systemic metabolic factors. These results indicate that the renal injury observed in *Ezh2* CKO diabetic mice is, at least in part, a direct consequence of the loss of tubular EZH2 mediated protection against hyperglycemia induced cellular stress.

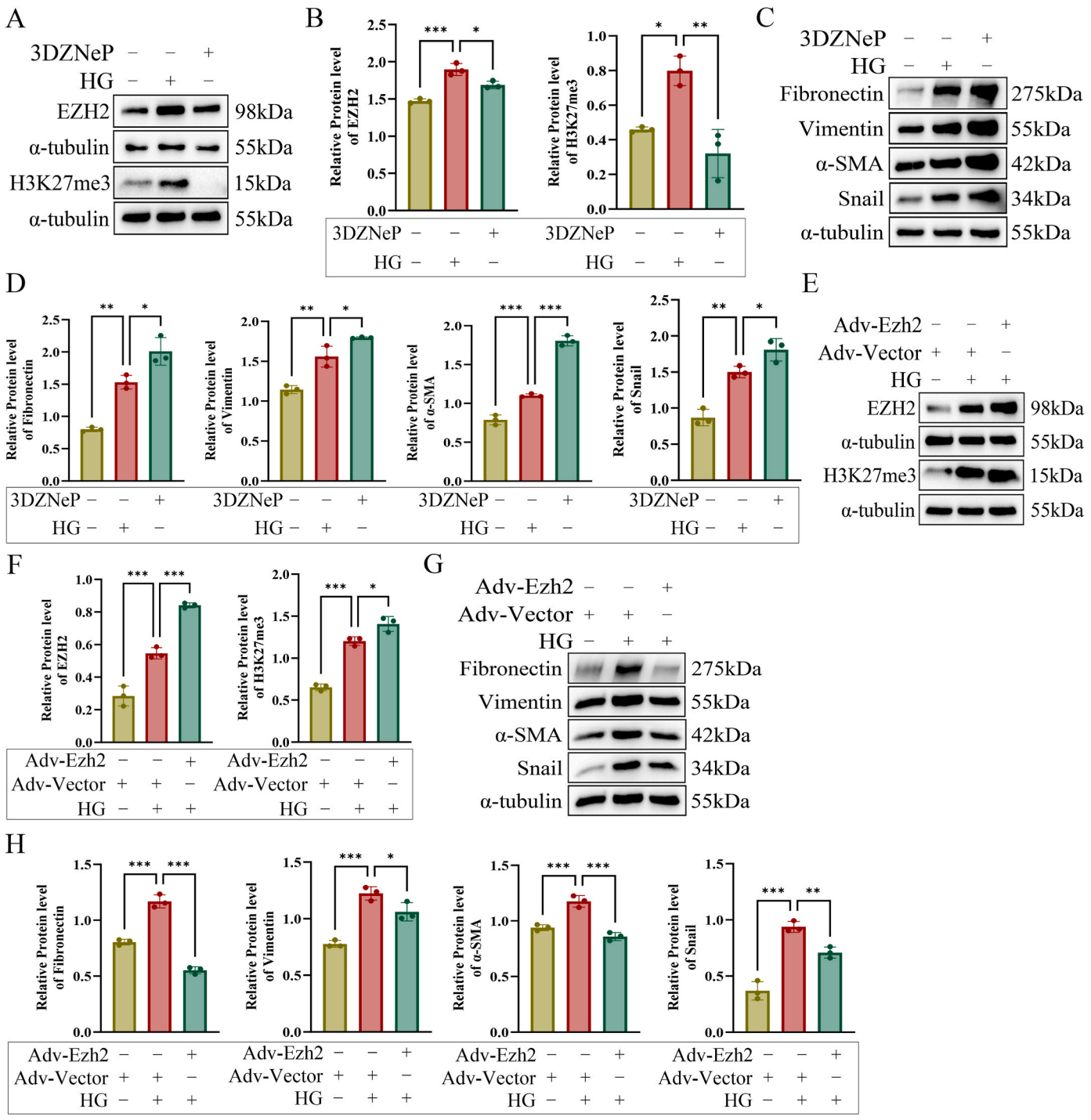



**Fig. 2.** EZH2 inhibits fibrotic responses in high glucose-stimulated renal epithelial cells
(A-D) Western blot analysis and quantification of EZH2, H3k27me3 and fibrotic markers (fibronectin, E-cadherin, vimentin, α-SMA) in HK2 cells stimulated with normal glucose (5.5 mM) or high glucose (30 mM) for 48 h. EZH2 was inhibited by 3DZNeP (1 μM) for 48 h. (E-H) EZH2 was overexpressed by adenovirus (Ad-EZH2) at a multiplicity of infection (MOI) of 10 in high glucose-stimulated HK2 cells for 48 h. Western blot analysis and quantification of EZH2, H3K27me3, and fibrotic markers. One representative of at least three independent experiments is shown. Data represent mean ± SD. *$p < 0.05$.**$p < 0.01$. ***$p < 0.001$.

Notably, tubular-specific Ezh2 deletion in non-diabetic mice did not result in significant renal dysfunction, histological abnormalities, or altered systemic glucose metabolism. This observation highlights that EZH2 functions primarily as a stress-responsive factor that is recruited under diabetic conditions to protect against injury, rather than as a constitutive homeostatic regulator under normal physiological conditions. This stress-inducible characteristic makes EZH2 an attractive therapeutic target—its modulation would likely not interfere with normal renal function while providing protection under pathological conditions.

The classic rodent model of DKD, induced by streptozotocin alone, frequently exhibits mild renal injury phenotypes, a protracted disease course, and limited tubulointerstitial fibrosis within a reasonable experimental timeframe [24]. To accelerate disease progression and better recapitulate the clinical presentation of advanced DKD with reduced nephron mass, we employed a dual-insult approach combining

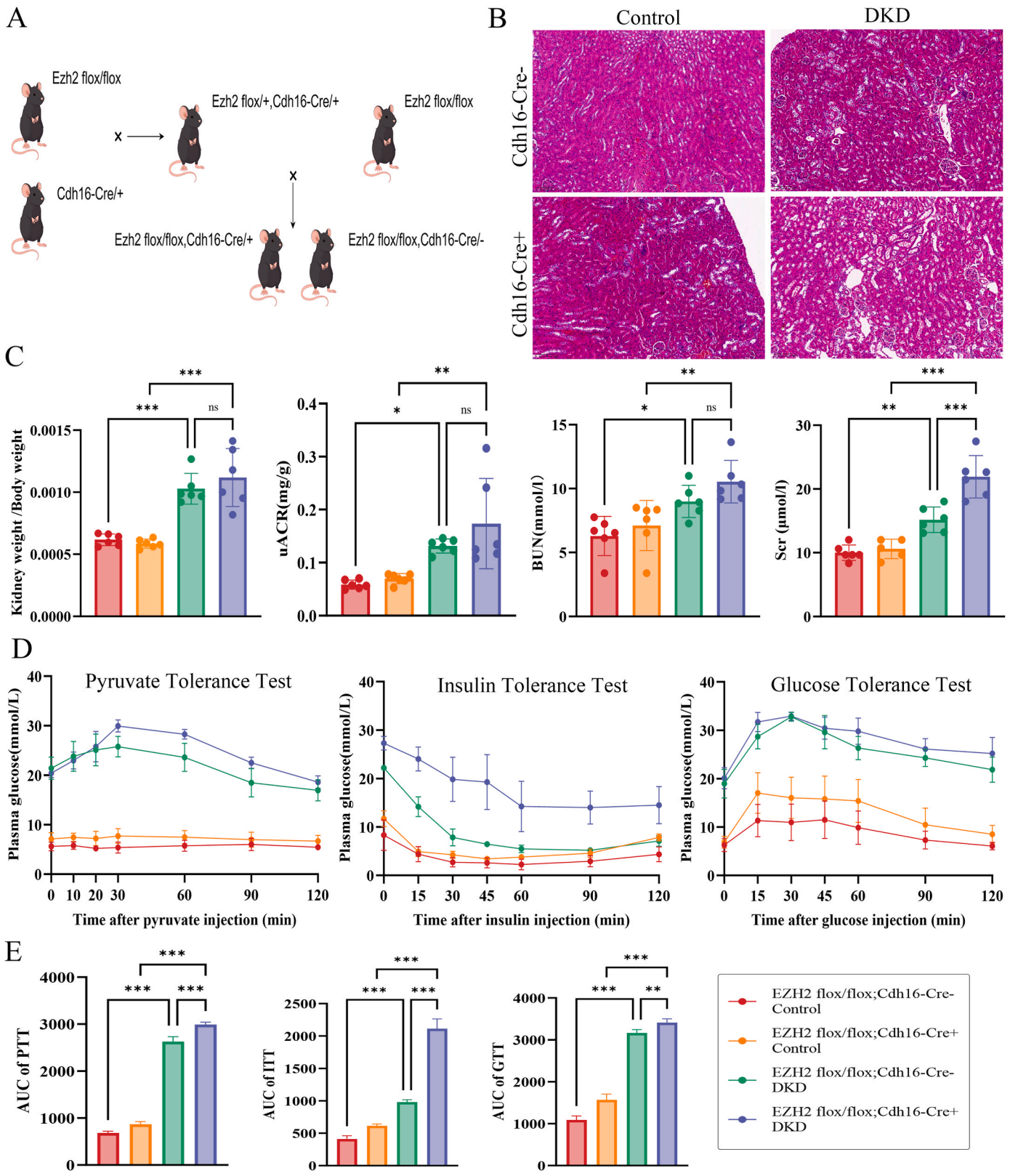



**Fig. 3.** Tubular deletion of *Ezh2* exacerbates disease progression in STZ-induced diabetic mice
(A) Mice with tubular specific deletion of *Ezh2* (*Ezh2* CKO) were established by crossing *Ezh2*$^{flox/flox}$ mice with Cdh16-cre mice. Diabe bic nephropathy was induced through STZ injection in mice with unilateral nephrectomy, which were fed with high fat diet (n = 6 per group). (B) HE staining (200× magnification) were performed to evaluate renal damages in control and diabetic mice. (C) Blood urea nitrogen (BUN) and serum creatinine (CREA) levels, urine albumin-creatinine ratio (uACR), and kidney/body weight ratio were analyzed. (D-E) Pyruvate tolerance test (PTT), insulin tolerance test (ITT) and glucose tolerance test (GTT) were performed to assess systemic glucose metabolism in mice. Area under the curve (AUC) following these tests were calculated. Data represent mean ± SD. *p < 0.05. **p < 0.01. ***p < 0.001.

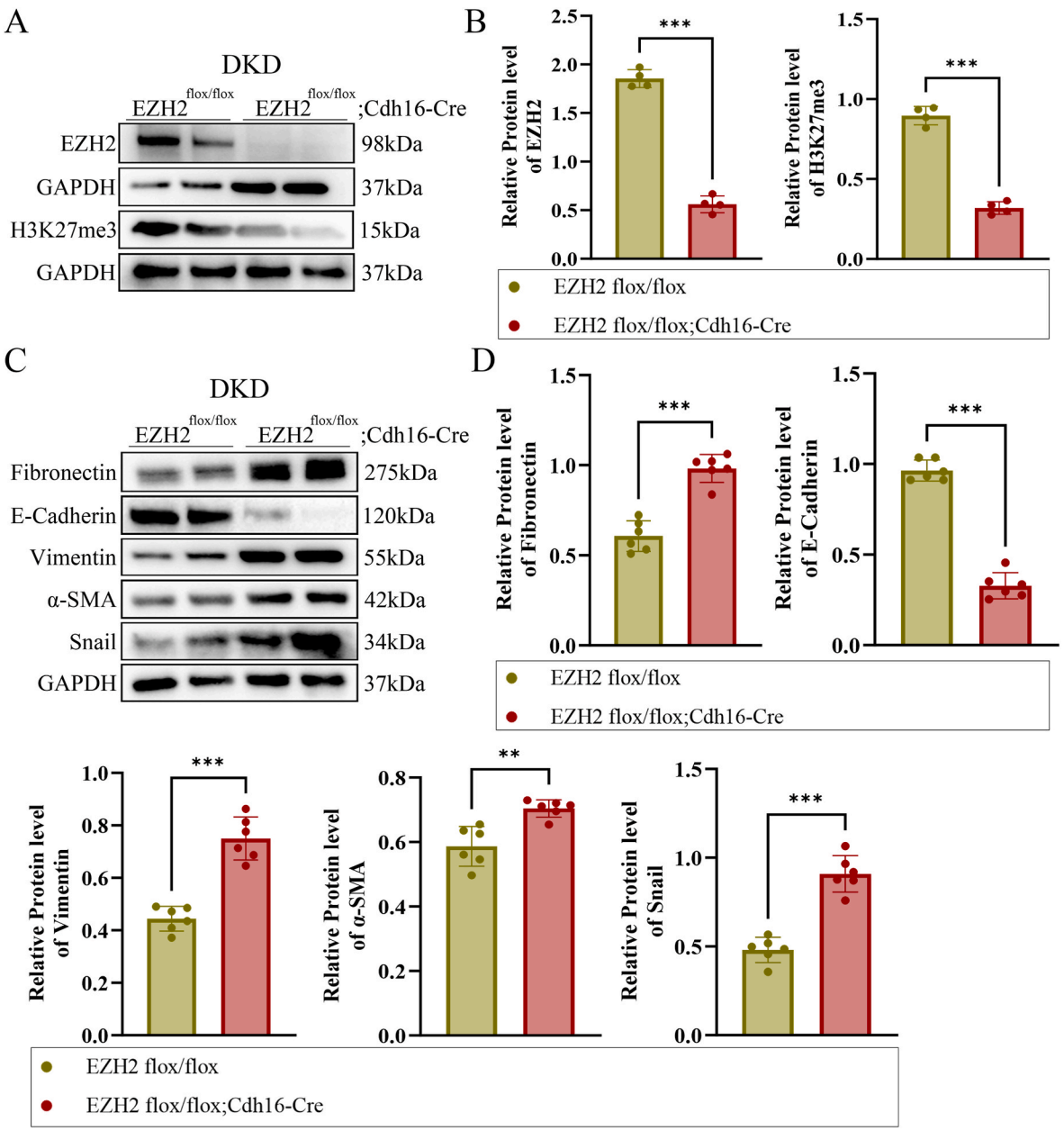



**Fig. 4.** Tubular deletion of *Ezh2* promotes renal fibrosis in STZ-induced diabetic mice
(A) Western blot analysis and quantification of EZH2 and H3K27me3 in kidney tissues from *Ezh2* $^{flox/flox}$ and *Ezh2* $^{flox/flox}$; cdh16-cre (*Ezh2* CKO) diabetic mice. (B) Western blot analysis and quantification of fibrotic markers (fibronectin, E-cadherin, vimentin, α-SMA, and Snail) in *Ezh2* $^{flox/flox}$ and *Ezh2* CKO diabetic kidneys. One representative of at least three independent experiments is shown. Data represent mean ± SD. **p < 0.01. ***p < 0.001.

hyperglycemia with unilateral nephrectomy [24,25]. Unilateral nephrectomy triggers compensatory hyperfiltration and increased tubular workload in the remnant kidney, thereby amplifying hyperglycemia-induced tubular injury signals and enabling evaluation of EZH2's role in DKD tubular injury within a feasible experimental window [25]. This model has been extensively validated for investigating DKD pathophysiological mechanisms [26,27]. Future studies utilizing alternative animal models that replicate early- or late-stage diabetic nephropathy will further enhance the clinical translatability of our findings.

Our study has another limitation. While our conclusions are strongly supported by data from animal and cellular models, clinical validation is still needed. Although we observed an inverse correlation between renal EZH2 expression and renal function in patients with DKD, the translational significance of these observations needs to be confirmed in larger human cohorts.

In conclusion, our study reveals that tubular EZH2 plays a protective role in DKD by inhibiting SHC1-mediated oxidative stress (Fig. 8). These results provide new insights into the pathogenesis of diabetic tubulopathy and suggest that maintaining or enhancing tubular EZH2 activity could represent a promising therapeutic strategy for DKD.

## 4. Materials and methods

### 4.1. Reagents

Streptozotocin (STZ; Cat# 18883-66-4) was purchased from Sigma-Aldrich. 3-Deazaneplanocin A (3DZNep; Cat# 102052-95-9, purity 99.80%) was obtained from MedChemExpress (Monmouth Junction, NJ, USA). Sodium pyruvate (Cat# A100342) was bought from Shanghai

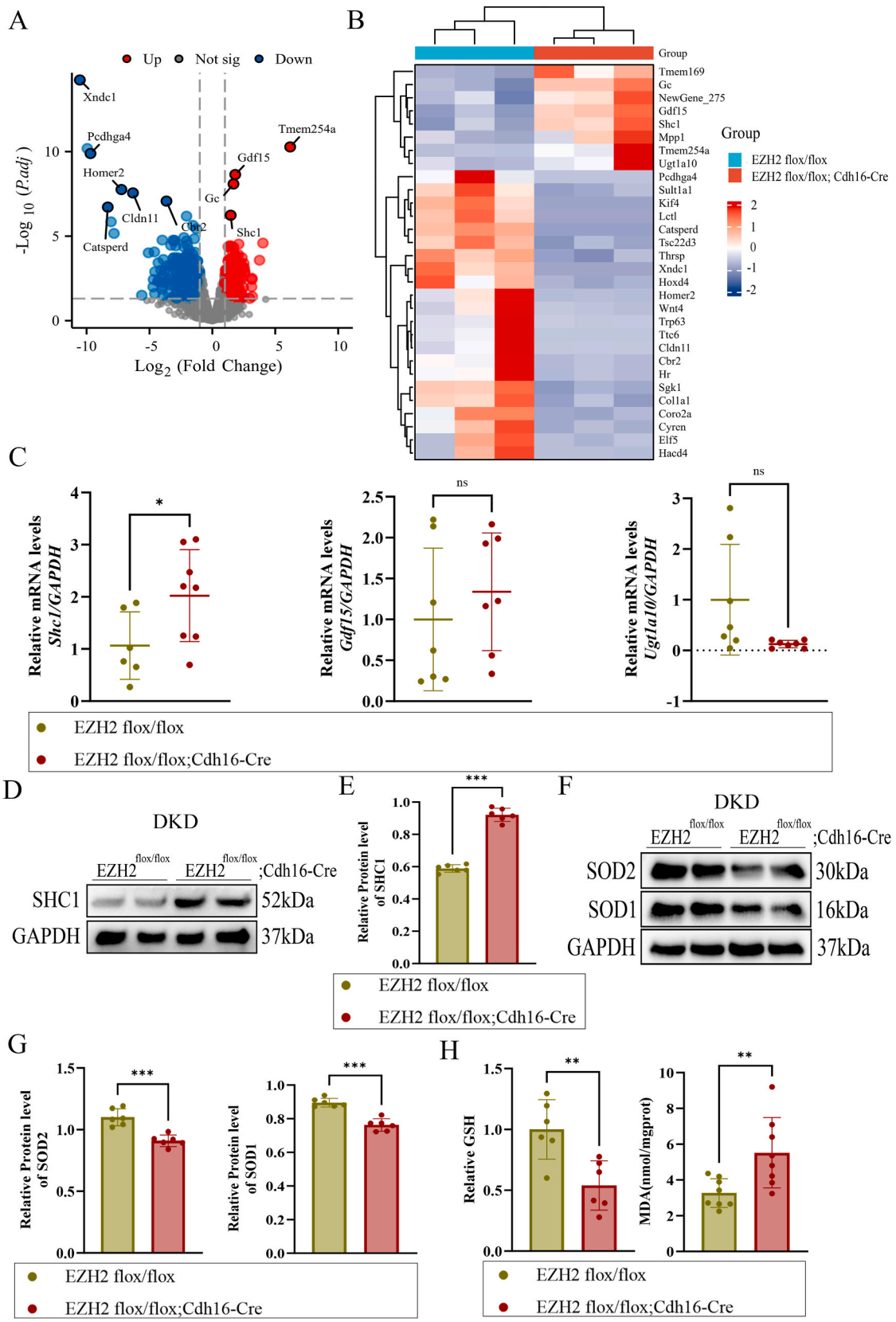



**Fig. 5.** Tubular deletion of *Ezh2* promotes oxidative stress in diabetic kidneys
(A) RNA-seq was performed in *Ezh2* WT vs. CKO diabetic kidneys. Volcano plot of RNA-seq data showing differential expressed genes (208 downregulated, 95 upregulated) between these two groups. (B) Heat map of top differential expressed genes ranked by p value between these two groups. (C) qPCR validation of three oxidative stress related genes in WT and *Ezh2* CKO diabetic kidneys. (D-F) Western blot analysis and quantification of SHC1, SOD1 and SOD2 expression in mouse kidneys. (G) Renal glutathione (GSH) and malondialdehyde (MDA) levels were measured in WT and *Ezh2* CKO diabetic kidneys. One representative of at least three independent experiments is shown. Data represent mean ± SD. Ns present not significant. *p < 0.05.**p < 0.01. ***p < 0.001.

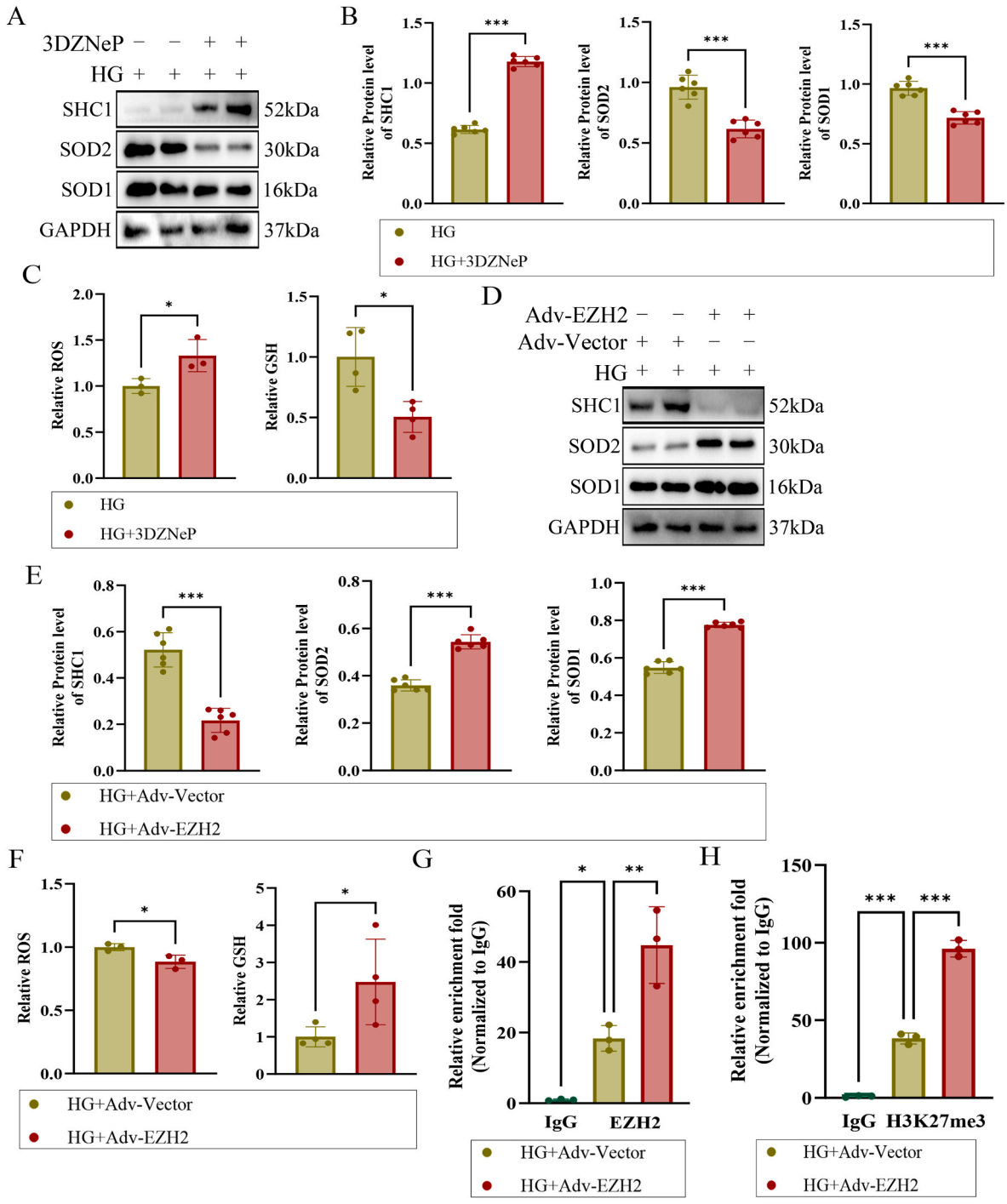



**Fig. 6.** EZH2 inhibits oxidative stress in high glucose-stimulated renal epithelial cells
High glucose-stimulated HK2 cells were treated with 1 μM 3DZNeP for 48 h. (A-B) Western blot analysis and quantification of SHC1, SOD1, and SOD2 in high glucose-treated HK2 cells. (C) Intracellular ROS and GSH levels were measured in HK2 cells. EZH2 was overexpressed in high glucose-stimulated HK2 cells through adenovirus (Ad-EZH2) at MOI of 10 for 48 h. (D-E) Western blot analysis and quantification of SHC1, SOD1, and SOD2 in high glucose-treated HK2 cells. (F) Intracellular ROS and GSH levels were measured in high glucose-stimulated HK2 cells with Ad-EZH2. (G-H) EZH2 and H3K27me3 occupancy on the SHC1 promoter in high glucose-stimulated HK-2 cells were analyzed by CUT&Tag qPCR. IgG severed as the negative control. One representative of at least three independent experiments is shown. Data represent mean ± SD. *p < 0.05. ***p < 0.001.

Shengong Biotechnology Co., Ltd. Shanghai, China. Assay kits for malondialdehyde (MDA), reactive oxygen species (ROS), glutathione (GSH), serum creatinine (Scr), and blood urea nitrogen (BUN) were purchased from the Nanjing Jiancheng Bioengineering Institute (Nanjing, China).

### 4.2. Animal experiments

All animal procedures and experimental protocols were performed in compliance with the guidelines approved by the Animal Ethics Committee of Shanghai University of Traditional Chinese Medicine (Approval No. PZSHUCTM250626003). *Ezh2* $^{flox/flox}$ (*Ezh2* $^{f/f}$) mice on a C57BL/6 background were kindly provided by Prof. Xi Wang from

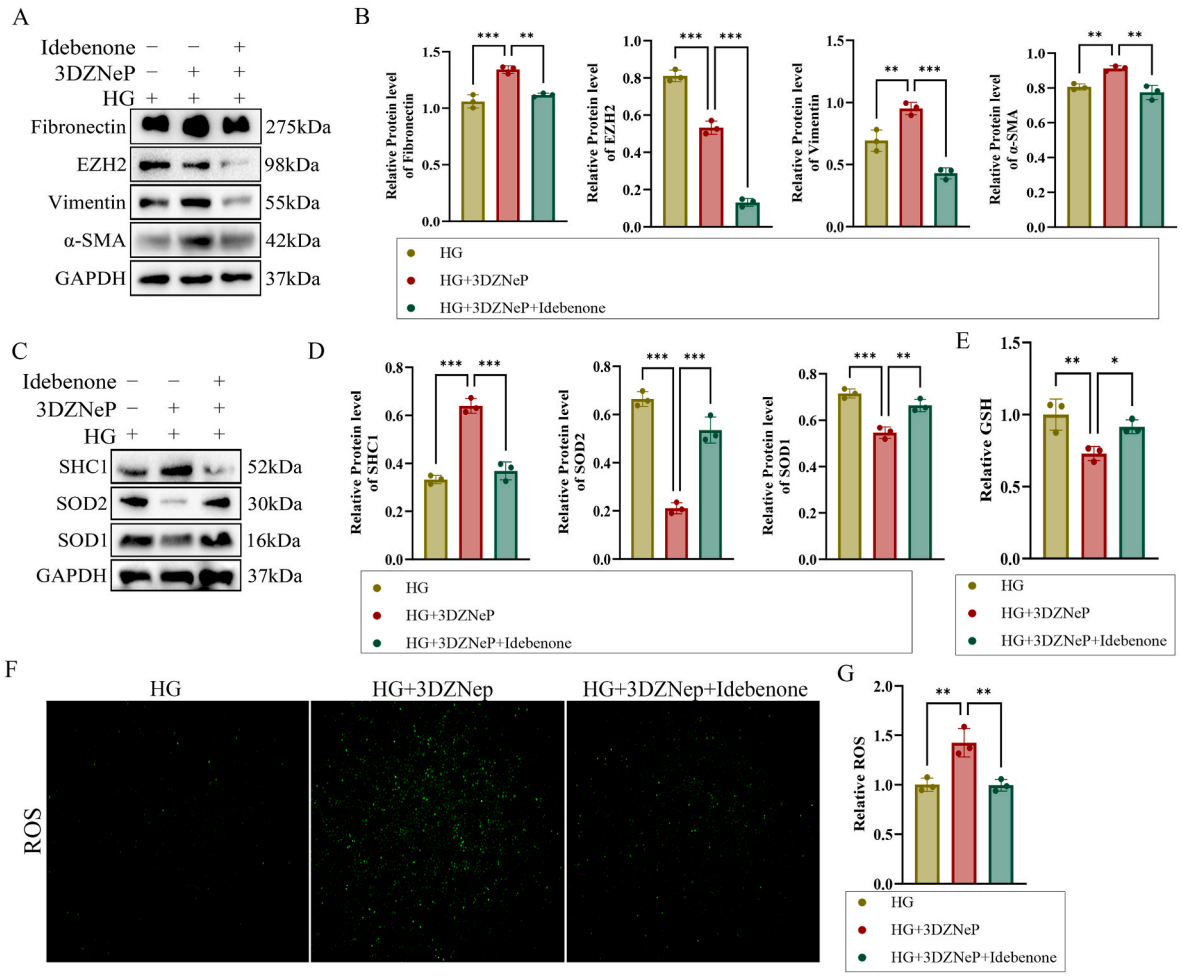



**Fig. 7.** EZH2 attenuates fibrotic responses through inhibition of SHC1
High glucose-stimulated HK2 cells were treated with 1 μM 3DZNeP in the presence or absence of SHC1 inhibitor idebenone (50 μM) for 48 h. (A-B) Western blot analysis and quantification of EZH2 and fibrotic markers (fibronectin, vimentin, and α-SMA). (C-D) Western blot analysis and quantification of SHC1, SOD1 and SOD2. (E-G) Intracellular GSH and ROS levels in high glucose-stimulated HK2 cells were measured. One representative of at least three independent experiments is shown. Data represent mean ± SD. *p < 0.05.**p < 0.01. ***p < 0.001.

Capital Medical University [28]. These mice were crossed with Cdh16-Cre transgenic mice (stock no. 012237, Jackson Laboratory) to generate *Ezh2* $^{flox/+}$; Cdh16-Cre + heterozygotes. The heterozygotes were then backcrossed with *Ezh2* $^{flox/flox}$ mice to produce experimental group (*Ezh2* $^{flox/flox}$; Cdh16-Cre+) and littermate control group (*Ezh2* $^{flox/flox}$; Cdh16-Cre-). All mice were maintained on C57BL/6J background (backcrossed for at least 6 generations). *Ezh2* $^{flox/+}$ represents the first-generation heterozygous offspring used for breeding only; the final experimental and control groups are both *Ezh2* $^{flox/flox}$ homozygotes (with or without Cre recombinase). Animals were housed under controlled temperature conditions with a 12-h light/dark cycle and had ad libitum access to food and water.

The DKD mouse model was constructed according to a previous published protocol [27]. After one week of acclimatization, mice were randomly divided into four groups (n = 6 per group). Six mice served as the sham-operated control group, which received a standard diet. The remaining mice were assigned to the model (DKD) group and fed a high-sugar, high-fat diet (HSHFD; composition: 67% maintenance feed, 10% lard, 20% sucrose, 2.5% cholesterol, 0.5% sodium cholate), followed by unilateral left nephrectomy. After one week of post-operative recovery, and following a 12-h fast, diabetes was induced by a single intraperitoneal (i.p.) injection of STZ (50 mg/kg) dissolved in sodium citrate buffer (pH 4.5). The sham group received an equal volume of the citrate buffer vehicle. Four days post-injection, plasma glucose levels were measured for three consecutive days using blood collected from the tail vein with an Accu-Chek glucose meter (Roche Diagnostics, Indianapolis, IN, USA). A diabetic mouse model was considered established when plasma glucose levels were ≥16.7 mmol/L. The early-stage DKD model was defined based on the urine albumin-to-creatinine ratio (uACR), with 24-h urine collected using metabolic cages. Mouse health status and body weight were monitored regularly. Body weight and blood glucose were measured weekly. At the end of the 6-week experimental period, urine samples were collected. Mice were then anesthetized with sodium pentobarbital (50 mg/kg, i.p.), and samples (including blood and kidney tissues) were immediately collected for analysis.

### 4.3. Evaluation of biochemical data

BUN, Scr, and UACR levels were measured using an automatic biochemical analyzer (Model: TC6010 L; Tecom Science Corporation, Nanchang, Jiangxi, China) in accordance with standard clinical protocols at the Clinical Laboratory of Shuguang Hospital.

### 4.4. Mouse glucose tolerance test (GTT)

Following a 24-h fast, mice were injected intraperitoneally with glucose (0.5 g/kg body weight). Blood glucose levels were measured

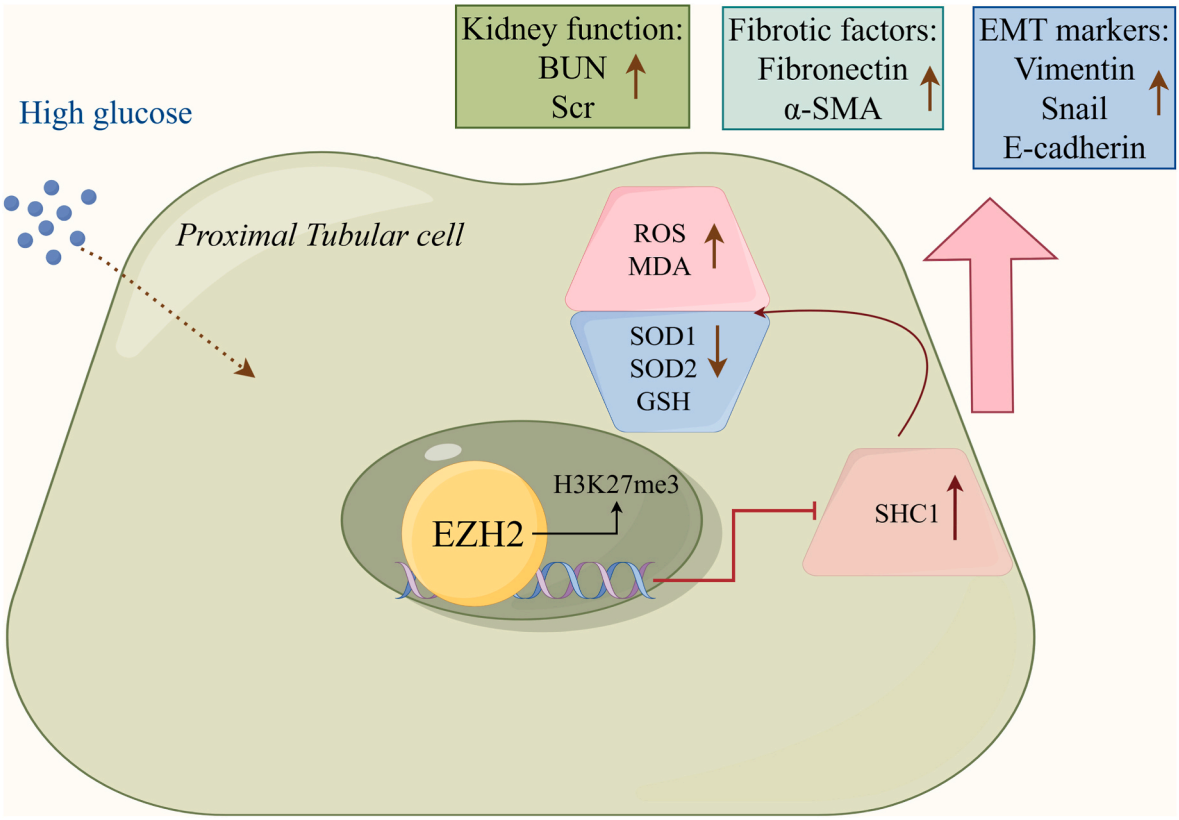



**Fig. 8.** Schematic illustration of the role of tubular EZH2 in hyperglycemia-induced kidney injury Under hyperglycemic conditions, EZH2 — predominantly expressed in renal tubules — is significantly upregulated. Tubular EZH2 exerts a protective effect against renal function decline and fibrosis in diabetic kidney disease by suppressing SHC1-mediated oxidative stress.

from tail vein blood using a glucose meter (Contour Next One; Bayer) immediately before (time = 0) and at 15, 30, 45, 60, 90, and 120 min after glucose injection. Food was provided to the mice at the end of the experiment, and changes in blood glucose at each time point were analyzed.

### 4.5. Mouse insulin tolerance test (ITT)

After an 8-h food restriction, mice were injected intraperitoneally with 0.5 U per kg body weight of human recombinant insulin (Sigma). Blood glucose was measured before (time = 0) and at 15, 30, 45, 60, 90, and 120 min after insulin injection. If blood glucose dropped below 2 mM, mice were rescued by i.p. injection of 30 mg glucose and excluded from the analysis.

### 4.6. Mouse pyruvate tolerance test (PTT)

Fasting was initiated at 4:00 p.m. on the day before the experiment and continued for 16 h. Water was provided ad libitum during fasting to maintain normal physiological status. The experiment started at 8:00 a.m. the next day. Baseline fasting blood glucose levels were measured using a glucose meter with compatible test strips. Sodium pyruvate was diluted in phosphate-buffered saline (PBS) and administered intraperitoneally at a dose of 2 g/kg. Blood glucose levels were measured and recorded at 10, 20, 30, 60, 90, and 120 min post-injection. Food was provided to the mice at the end of the experiment.

### 4.7. Renal histological examination

Kidney tissues were fixed in 10% neutral buffered formalin, embedded in paraffin, and sectioned at a thickness of 4 μm. After deparaffinization and rehydration, kidney sections were stained with Hematoxylin and Eosin (H&E; D006-1-1, Jiancheng, Nanjing, China). Sections were observed under an optical microscope at 200× magnification, and images were captured using a Leica SCN400 slide scanning system and its accompanying software. Tubular injury was assessed in a double-blinded manner and graded based on the severity of damage.

### 4.8. Immunofluorescence staining

Paraffin-embedded kidney sections (4 μm) were subjected to antigen retrieval using sodium citrate buffer, followed by permeabilization with 0.5% Triton X-100 and blocking with 5% bovine serum albumin (BSA). Sections were then incubated overnight at 4°C with rabbit anti-EZH2 (D2C9, Cell Signaling Technology, 1:200) and mouse anti-LRP2 (HA722151, HUABIO, 1:200) antibodies. On the following day, sections were incubated with horseradish peroxidase (HRP)-conjugated goat anti-rabbit IgG (1:10,000; Biosynthesis Biotechnology Co., Ltd., Beijing, China) at room temperature for 1 h in the dark. After nuclear counterstaining with DAPI, sections were mounted and imaged using a confocal microscope.

### 4.9. Cell culture

Human Kidney 2 (HK2) cells, a human renal proximal tubular epithelial cell line, were purchased from the Cell Bank of the Shanghai Institute of Biological Sciences, Chinese Academy of Sciences (Shanghai, China). HK2 cells were cultured in DMEM medium (Gbico, Cat: 11885) containing 10% fetal bovine serum (FBS) and 0.5% penicillin/streptomycin at 37°C in a 5% CO2 atmosphere. Cells were seeded into six-well plates. When cell density reached approximately 50%, they were treated for 24 h with media containing normal glucose (NG; 5.5 mM D-glucose

+ 24.5 mM mannitol) or high glucose (HG; 30 mM D-glucose). Cell culture supernatants and cellular proteins were collected for subsequent analysis after 24 h. Cellular proteins were also collected after 48 h of treatment for further analysis.

For overexpression experiments, recombinant adenoviral vectors encoding human full-length EZH2 (Adv-EZH2, Vigene Biosciences, Jinan, China) were used. Empty adenoviral vectors (Adv-Vector) served as negative controls. HK2 cells were seeded into six-well plates and infected with adenovirus at a multiplicity of infection (MOI) of 10 when cell confluence reached approximately 50%. The culture medium was replaced 4 h post-infection. Cells were harvested 48 h after infection for protein extraction and subsequent analysis.

### 4.10. GSH and MDA assays

Kidney tissues and HK2 cells were homogenized in lysis buffer and centrifuged at 12,000 g for 10 min at 4°C. The resulting supernatants were collected, and the levels of GSH and MDA were determined using commercial assay kits (A006-2-1 for GSH, A003-1 for MDA; Jiancheng, Nanjing, China) according to the manufacturer's instructions.

### 4.11. Detection of ROS

Intracellular ROS levels in HK2 cells were measured using the DCFH-DA fluorescent probe (ROS Assay Kit, Cat. No. S0033S, Beyotime Biotechnology, Shanghai, China). In brief, cells were loaded with 10 μmol/L DCFH-DA and incubated at 37°C for 30 min. After washing three times with phosphate-buffered saline (PBS), fluorescence intensity was quantified using a microplate reader (Biotek, USA) with excitation at 488 nm and emission at 525 nm. For morphological assessment of ROS production, cells were visualized and imaged under a fluorescence microscope (TH4-200, Olympus, Japan) with consistent imaging parameters applied to all experimental groups.

### 4.12. Quantitative PCR (qPCR) analysis

Kidney tissue samples were collected, immediately snap-frozen in liquid nitrogen to preserve RNA integrity, and stored at −80°C until processing. Total RNA was extracted using TRIzol reagent (CW0580S; JiangSu CoWin Biotec, Beijing, China) according to the manufacturer's instructions. cDNA was synthesized using the Evo M-MLV RT Premix kit (AG11706; Accurate Biology, China). Quantitative real-time PCR was performed using the SYBR Green Premix Pro Taq HS qPCR Kit (AG11701; Accurate Biology, China) on an ABI 7500 PCR system (Applied Biosystems, Waltham, MA, USA). The relative expression levels of target genes were calculated using the $2^{-\Delta\Delta Ct}$ method, normalized to the expression of glyceraldehyde-3-phosphate dehydrogenase (GAPDH). All experiments were performed in triplicate. The primer sequences for qPCR were listed in Table S1.

### 4.13. Western blotting analysis

Renal cortex tissues were dissected from mice and homogenized in radioimmunoprecipitation assay (RIPA) lysis buffer (P0013B, Beyotime Biotechnology, China). After centrifugation at 13,000 rpm for 15 min at 4°C, the supernatant was collected. Protein concentration was determined using a bicinchoninic acid (BCA) protein assay kit (Beyotime Biotechnology Institute). Protein lysates were separated by 10–12% SDS-polyacrylamide gel electrophoresis (SDS-PAGE) and transferred onto polyvinylidene fluoride (PVDF) membranes (0.2 μm, Bio-Rad Laboratories, Inc.). Membranes were blocked with 5% (w/v) non-fat milk in Tris-buffered saline containing 0.1% Tween-20 (TBS-T) for 1 h at room temperature and then incubated with the designated primary antibodies overnight at 4°C. The primary antibodies used in this study were as follows: GAPDH (6004-1-1g, Proteintech, 1:5000), EZH2 (D2C9, Cell Signaling Technology, 1:1000), Fibronectin (ab45688, Abcam, 1:2500), α-Smooth Muscle Actin (α-SMA; ET1607-53, HUABIO, 1:2000), Snail (A11794, ABclonal, 1:2000), SHC1 (EM1706-40, HUABIO, 1:1000), SOD1 (A0274, ABclonal, 1:1000), SOD2 (A1340, ABclonal, 1:1000), Histone H3 trimethyl Lys27 (H3K27me3; ab192985, Abcam, 1:1000), Vimentin (ET1610-39, HUABIO, 1:5000), and alpha-Tubulin (ET1705-31, HUABIO, 1:5000). After washing three times with PBS-T at 5-min intervals, the membranes were incubated with horseradish peroxidase (HRP)-conjugated goat anti-rabbit IgG (1:10,000 dilution; Biosynthesis Biotechnology Co., Ltd., Beijing, China) or goat anti-mouse IgG (1:10,000 dilution; Biosynthesis Biotechnology Co., Ltd., Beijing, China) for 1 h at room temperature. Immunoreactive bands were visualized using Immobilon Western Chemiluminescent HRP Substrate (Millipore Corporation, Billerica, MA, USA) and a Bio-Rad ChemiDoc MP Imaging System. Densitometric analysis was conducted using ImageJ software version 6.0 (National Institutes of Health, Bethesda, MD, USA).

### 4.14. RNA sequencing analysis

High-throughput RNA sequencing was employed to investigate gene expression patterns and obtain precise digital gene expression profiles. RNA samples underwent standard library preparation procedures, which included mRNA enrichment using oligo(dT) magnetic beads, RNA fragmentation, first-strand cDNA synthesis, second-strand cDNA synthesis, adapter ligation, and PCR amplification. The resulting circularized DNA libraries were sequenced. Raw sequencing data were subjected to stringent quality control to generate high-quality clean data. Subsequent comprehensive analysis, including read alignment, and gene expression quantification, was performed using integrated multi-omics data mining systems. Differentially expressed genes were calculated by DESeq2_EBSeq algorithms with FDR (False Discovery Rate) $\leq 0.05$ and fold-change $>2$.

### 4.15. Bioinformatics analysis

Gene expression datasets from Ju CKD TubInt (RNA-seq) and GSE30122 (Affymetrix microarray) were retrieved from the Nephroseq v5 database (https://nephroseq.com; University of Michigan, Ann Arbor, MI, USA). Nephroseq v5 is a specialized integrative platform for kidney disease transcriptomics, where all raw data undergo standardized preprocessing according to established protocols. Specifically, the Ju CKD TubInt dataset was normalized using the median-of-ratios method implemented in DESeq2, while the GSE30122 dataset was processed with the Robust Multi-array Average (RMA) algorithm for background correction and quantile normalization. Preprocessed expression matrices and differential expression analysis results were directly downloaded from the platform. Differentially expressed genes were defined as those with $|\log_2 \text{fold change}| > 1$ and $P < 0.05$ (unadjusted P values, as per platform default settings).

Humphreys lab single-nucleus RNA sequencing (snRNA-seq) data were obtained from the KIT (Kidney Interactive Transcriptomics) database (http://humphreyslab.com/SingleCell/; RRID: SCR_017209). KIT is an online analytical platform developed by the Humphreys Laboratory at Washington University School of Medicine, integrating multiple published kidney single-cell and single-nucleus RNA-seq datasets encompassing healthy kidney, diabetic kidney disease, and kidney injury conditions. The Comparative Analysis module was utilized to interrogate EZH2 expression distribution across renal cell subpopulations. Single-cell data provided by the platform were preprocessed using LogNormalize (scaling total cellular counts to 10,000 per cell). Cell clustering was performed based on t-distributed stochastic neighbor embedding (t-SNE)/uniform manifold approximation and projection (UMAP) dimensionality reduction and Louvain community detection algorithm, with cell type annotations assigned according to established marker genes from published literature.

### 4.16. Cleavage Under Targets and Tagmentation (CUT&Tag) qPCR

CUT&Tag assays were performed according to the manufacturer's protocol using the Hyperactive® In-Situ ChIP Library Prep Kit for Illumina® (HD101-01, Vazyme Biotech, Nanjing, China). Briefly, $1 \times 10^5$ HK2 cells were bound to concanavalin A (ConA)-coated magnetic beads and incubated overnight at 4°C with EZH2 antibody (D2C9, Cell Signaling Technology, 1:100), H3K27me3 antibody (HA722376, HUABIO, 1:100), or rabbit IgG isotype control (1:100). Protein A/G-MNase fusion protein was subsequently added and incubated at room temperature for 1 h. Targeted chromatin cleavage was activated by adding $CaCl_2$ (37°C, 30 min). After terminating the reaction, DNA was extracted and subjected to quantitative PCR analysis. Primer sequences for the *SHC1* promoter region were: forward, 5′-CCCCAGACTCAGGACTCAGA-3'; reverse, 5′-TCAGCCTCCTGGGTAGGTAG-3'. Enrichment was calculated as percentage of input DNA and normalized to IgG control. Data are expressed as mean ± SD from three independent experiments.

### 4.17. Statistical analysis

Statistical comparisons between two groups were performed using either the parametric Student's t-test or the non-parametric Mann-Whitney *U* test, depending on the data distribution. Comparisons among multiple groups were conducted using one-way analysis of variance (ANOVA) or the Kruskal-Wallis test. All statistical analyses were performed using GraphPad Prism 9 (GraphPad Software, San Diego, CA, USA) or R software. A P-value of less than 0.05 was considered statistically significant.

## Statements and declarations

The authors declare that they have no known competing financial interests or personal relationships that could have appeared to influence the work reported in this paper.

## Data availability statement

The data analyzed during this study are included in this article. Additional supporting data are available from the corresponding authors upon reasonable request.

## Funding

This work was supported by Shanghai, PR China; Scientific Research Foundation of Shanghai Municipal Commission of Health and Family Planning (201740193) to MW; National Natural Science Foundation of China (82274492) and Shanghai Municipal Science and Technology Commission - Scientific Research Program Projects (22Y31920200) to XY, National Natural Science Foundation of China (82474269) and the Western Medicine Guiding Project of Shanghai Science and Technology Commission (18411961000) to DC, National Natural Science Foundation of China (82305095) to PL, Pudong New Area Health Commission Health Planning and Research Project Plan (PW2022D-12) and Construction Plan for the Pilot Project on the Inheritance and Innovative Development of Traditional Chinese Medicine in Pudong New Area (YC-2023-0602) to JH.

## CRediT authorship contribution statement

**Qiming Xu:** Data curation, Investigation. **Pinglan Lin:** Data curation, Investigation. **Sijun Chen:** Data curation, Investigation. **Jianrao Lu:** Data curation, Investigation. **Lin Li:** Conceptualization, Writing – original draft, Writing – review & editing. **Reza Moghadasali:** Data curation, Investigation. **Xuejun Yang:** Conceptualization, Writing – original draft, Writing – review & editing. **Jing Hu:** Conceptualization, Data curation, Formal analysis, Funding acquisition, Methodology, Resources, Software, Writing – original draft, Writing – review & editing. **Ming Wu:** Conceptualization, Data curation, Formal analysis, Funding acquisition, Methodology, Resources, Software, Writing – original draft, Writing – review & editing. **Dongping Chen:** Conceptualization, Formal analysis, Funding acquisition, Methodology, Resources, Software, Writing – original draft, Writing – review & editing.

## Competing interests

The authors have no competing interest to declare.

## Appendix A. Supplementary data

Supplementary data to this article can be found online at https://doi.org/10.1016/j.freeradbiomed.2026.08.019.

## References

[1] E. Mlynarska, D. Bulawska, W. Czarnik, J. Hajdys, G. Majchrowicz, F. Prusinowski, M. Stabrawa, J. Rysz, B. Franczyk, Novel insights into diabetic kidney disease, Int. J. Mol. Sci. 25 (18) (2024).
[2] K.R. Tuttle, G.L. Bakris, R.W. Bilous, J.L. Chiang, I.H. de Boer, J. Goldstein-Fuchs, I. B. Hirsch, K. Kalantar-Zadeh, A.S. Narva, S.D. Navaneethan, J.J. Neumiller, U. D. Patel, R.E. Ratner, A.T. Whaley-Connell, M.E. Molitch, Diabetic kidney disease: a report from an ADA Consensus Conference, Diabetes Care 37 (10) (2014) 2864–2883.
[3] H. Sun, P. Saeedi, S. Karuranga, M. Pinkepank, K. Ogurtsova, B.B. Duncan, C. Stein, A. Basit, J.C.N. Chan, J.C. Mbanya, M.E. Pavkov, A. Ramachandaran, S.H. Wild, S. James, W.H. Herman, P. Zhang, C. Bommer, S. Kuo, E.J. Boyko, D.J. Magliano, IDF Diabetes Atlas: global, regional and country-level diabetes prevalence estimates for 2021 and projections for 2045, Diabetes Res. Clin. Pract. 183 (2022) 109119.
[4] R.E. Gilbert, Proximal tubulopathy: prime mover and key therapeutic target in diabetic kidney disease, Diabetes 66 (4) (2017) 791–800.
[5] R. Haraguchi, Y. Kohara, K. Matsubayashi, R. Kitazawa, S. Kitazawa, New insights into the pathogenesis of diabetic nephropathy: proximal renal tubules are primary target of oxidative stress in diabetic kidney, Acta Histochem. Cytoc. 53 (2) (2020) 21–31.
[6] J. Slyne, C. Slattery, T. McMorrow, M.P. Ryan, New developments concerning the proximal tubule in diabetic nephropathy: in vitro models and mechanisms, Nephrol. Dial. Transplant. 30 (Suppl 4) (2015) iv60–i67.
[7] V. Vallon, S.C. Thomson, Renal function in diabetic disease models: the tubular system in the pathophysiology of the diabetic kidney, Annu. Rev. Physiol. 74 (2012) 351–375.
[8] T. Li, C. Yu, S. Zhuang, Histone methyltransferase EZH2: a potential therapeutic target for kidney diseases, Front. Physiol. 12 (2021) 640700.
[9] R. Cao, L. Wang, H. Wang, L. Xia, H. Erdjument-Bromage, P. Tempst, R.S. Jones, Y. Zhang, Role of histone H3 lysine 27 methylation in Polycomb-group silencing, Science 298 (5595) (2002) 1039–1043.
[10] F.S. Siddiqi, S. Majumder, K. Thai, M. Abdalla, P. Hu, S.L. Advani, K.E. White, B. B. Bowskill, G. Guarna, C.C. Dos Santos, K.A. Connelly, A. Advani, The histone methyltransferase enzyme enhancer of zeste homolog 2 protects against podocyte oxidative stress and renal injury in diabetes, J. Am. Soc. Nephrol. 27 (7) (2016) 2021–2034.
[11] Y. Jia, M.A. Reddy, S. Das, H.J. Oh, M. Abdollahi, H. Yuan, E. Zhang, L. Lanting, M. Wang, R. Natarajan, Dysregulation of histone H3 lysine 27 trimethylation in transforming growth factor-beta1-induced gene expression in mesangial cells and diabetic kidney, J. Biol. Chem. 294 (34) (2019) 12695–12707.
[12] X. Zhou, X. Zang, M. Ponnusamy, M.V. Masucci, E. Tolbert, R. Gong, T.C. Zhao, N. Liu, G. Bayliss, L.D. Dworkin, S. Zhuang, Enhancer of zeste homolog 2 inhibition attenuates renal fibrosis by maintaining smad7 and phosphatase and tensin homolog expression, J. Am. Soc. Nephrol. 27 (7) (2016) 2092–2108.
[13] G. Biondi, N. Marrano, A. Borrelli, M. Rella, R. D'Oria, V.A. Genchi, C. Caccioppoli, A. Cignarelli, S. Perrini, L. Laviola, F. Giorgino, A. Natalicchio, The p66(Shc) redox protein and the emerging complications of diabetes, Int. J. Mol. Sci. 25 (1) (2023).
[14] F. Bock, K. Shahzad, H. Wang, S. Stoyanov, J. Wolter, W. Dong, P.G. Pelicci, M. Kashif, S. Ranjan, S. Schmidt, R. Ritzel, V. Schwenger, K.G. Reymann, C. T. Esmon, T. Madhusudhan, P.P. Nawroth, B. Isermann, Activated protein C ameliorates diabetic nephropathy by epigenetically inhibiting the redox enzyme p66Shc, Proc. Natl. Acad. Sci. U. S. A. 110 (2) (2013) 648–653.
[15] S. Yang, L. Zhao, Y. Han, Y. Liu, C. Chen, M. Zhan, X. Xiong, X. Zhu, L. Xiao, C. Hu, F. Liu, Z. Zhou, Y.S. Kanwar, L. Sun, Probucol ameliorates renal injury in diabetic nephropathy by inhibiting the expression of the redox enzyme p66Shc, Redox Biol. 13 (2017) 482–497.
[16] M. Zhan, I. Usman, J. Yu, L. Ruan, X. Bian, J. Yang, S. Yang, L. Sun, Y.S. Kanwar, Perturbations in mitochondrial dynamics by p66Shc lead to renal tubular oxidative injury in human diabetic nephropathy, Clin. Sci. (Lond.) 132 (12) (2018) 1297–1314.
[17] S. Raez-Villanueva, A. Debnath, D.B. Hardy, A.C. Holloway, Prenatal nicotine exposure leads to decreased histone H3 lysine 9 (H3K9) methylation and increased

p66shc expression in the neonatal pancreas, J Dev Orig Health Dis 13 (2) (2022) 156–160.
[18] Y. Xiao, J. Xia, J. Cheng, H. Huang, Y. Zhou, X. Yang, X. Su, Y. Ke, W. Ling, Inhibition of S-Adenosylhomocysteine hydrolase induces endothelial dysfunction via epigenetic regulation of p66shc-Mediated oxidative stress pathway, Circulation 139 (19) (2019) 2260–2277.
[19] Y. Gu, Z. Wang, K. Wang, Y. Wang, Y. Li, S. Jiang, Y. Zheng, R. Feng, M. Yang, Low-dose valproic acid ameliorates osteoporosis by restoring redox homeostasis and suppressing ferritinophagy-dependent ferroptosis via EZH2/H3K27me3 signaling, Free Radic. Biol. Med. 241 (2025) 76–89.
[20] S. Oda, Y. Kato, M. Hatakeyama, A. Iwamura, T. Fukami, T. Kume, T. Yokoi, M. Nakajima, Evaluation of expression and glycosylation status of UGT1A10 in Supersomes and intestinal epithelial cells with a novel specific UGT1A10 monoclonal antibody, Drug Metab. Dispos. 45 (9) (2017) 1027–1034.
[21] A.M. di Candia, D.X. de Avila, G.R. Moreira, H. Villacorta, A.S. Maisel, Growth differentiation factor-15, a novel systemic biomarker of oxidative stress, inflammation, and cellular aging: potential role in cardiovascular diseases, Am. Heart J. 9 (2021) 100046.
[22] Y. Cheng, Y. Chen, G. Wang, P. Liu, G. Xie, H. Jing, H. Chen, Y. Fan, M. Wang, J. Zhou, Protein methylation in diabetic kidney disease, Front Med (Lausanne) 9 (2022) 736006.
[23] D. Legouis, A. Faivre, P.E. Cippa, S. de Seigneux, Renal gluconeogenesis: an underestimated role of the kidney in systemic glucose metabolism, Nephrol. Dial. Transplant. 37 (8) (2022) 1417–1425.
[24] A. Lee, Mouse models of diabetic complications: dissecting molecular mechanisms of disease progression, Front. Biosci. (Landmark Ed.) 31 (3) (2026) 45430.
[25] M. Uil, A.M.L. Scantlebery, L.M. Butter, P.W.B. Larsen, O.J. de Boer, J.C. Leemans, S. Florquin, J. Roelofs, Combining streptozotocin and unilateral nephrectomy is an effective method for inducing experimental diabetic nephropathy in the 'resistant' C57Bl/6J mouse strain, Sci. Rep. 8 (1) (2018) 5542.
[26] N.A. Gujarati, B.O. Frimpong, M. Zaidi, R. Bronstein, M.P. Revelo, J.D. Haley, I. Kravets, Y. Guo, S.K. Mallipattu, Podocyte-specific KLF6 primes proximal tubule CaMK1D signaling to attenuate diabetic kidney disease, Nat. Commun. 15 (1) (2024) 8038.
[27] L. Li, J. Li, R. Li, X. Zhao, Y. Chen, Y. Cai, Y. Yang, W. Wang, S. Zheng, L. Zhang, X. Liang, Podocyte RIPK3 deletion improves diabetic kidney disease by attenuating NF-kappaB p65 driven inflammation, Adv. Sci. (Weinh.) 12 (33) (2025) e03325.
[28] J. Yin, J.W. Leavenworth, Y. Li, Q. Luo, H. Xie, X. Liu, S. Huang, H. Yan, Z. Fu, L. Y. Zhang, L. Zhang, J. Hao, X. Wu, X. Deng, C.W. Roberts, S.H. Orkin, H. Cantor, X. Wang, Ezh2 regulates differentiation and function of natural killer cells through histone methyltransferase activity, Proc. Natl. Acad. Sci. U. S. A. 112 (52) (2015) 15988–15993.